The effect of clay on the thermal degradation of polyamide 6 in polyamide 6/clay nanocomposites

Bok Nam Jang, Charles A. Wilkie*

Department of Chemistry, Marquette University, P.O. Box 1881, Milwaukee, WI 53201, USA

Abstract

The degradation pathway of polyamide 6/clay nanocomposites was studied as a function of clay content. Well-dispersed polymer–clay nanocomposites can be easily obtained by simple melt blending between organically-modified clays and polyamide 6. Polyamide 6–clay nanocomposites exhibit a large reduction in the peak heat release rate, 60%, measured by cone calorimetry. There are no significant differences in the evolved products during thermal degradation of polyamide 6 and polyamide 6/clay nanocomposites in terms of composition and functionality. The main degradation pathway of polyamide 6 is aminolysis and/or acidolysis, primarily through an intra-chain reaction, producing ε-carprolactam, which is the monomer of polyamide 6. As the clay loading is increased, the relative quantity of ε-carprolactam in the evolved products decreases and the viscosity of the soluble solid residues increases. It is thought that inter-chain reactions become significant in the presence of clay because the degrading polymer chains are trapped in the gallery space of the clay during thermal degradation.

1. Introduction

Polymer–clay nanocomposites have drawn considerable attention, because the addition of small amounts clay (≤ 5 wt%) brings about a large enhancement in the mechanical properties, thermal and fire properties and barrier properties of the polymer [1–4]. Polyamide 6 (PA 6)–clay nanocomposites have been actively studied since their introduction by Kato and co-workers [5]. Kamigaito et al. at Toyota achieved high heat resistance as well as enhanced mechanical properties by forming well-dispersed clay layers in a polyamide 6 matrix via in situ polymerization [6–8]. A particularly important observation is that the heat distortion temperature was increased from 65 °C for the virgin polyamide 6 to 152–164 °C for the nanocomposites, without the loss of mechanical properties [9–11]. The gas barrier and water sorption properties of polyamide 6 were also improved by incorporating organically-modified clays [12,13]. Polyamide 6 can readily form nanocomposites by simple melt blending with organically-modified clays [14, 15]. The reduction in the peak heat release rate using a cone calorimeter, PHRR, is very large, typically about a 60% reduction is observed for polyamide 6–clay nanocomposites [16,17]. The measurement of PHRR is important in fire studies, because this gives a measure of the size of the fire.

Two mechanisms have been suggested for the reduction in the PHRR, barrier formation [18] and paramagnetic radical trapping [19]. The formation of a barrier should retard mass transfer of degrading polymer to the vapor phase and also serve to shield the underlying polymer from the external thermal radiation and both of these lead to a reduction in the peak heat release rate. X-ray photoelectron spectroscopy (XPS) measurements have been carried out [20–23] on polymer–clay nanocomposites and these have shown that the clay does accumulate at the surface during thermal degradation of the polymer. The second pathway for reduction in PHRR, radical trapping, appears to only be important when the clay loading is quite low and the amount is insufficient to produce a good barrier. Barrier formation is the accepted mechanism for the reduction in PHRR.

The thermal degradation pathway of virgin polyamide 6 has been studied extensively in the past [24–28]. The most dominant evolved product during thermal degradation is ε-caprolactam, while HCN, CO_2, CO, NH_3, H_2O and acrylonitrile are detected as trace products. The evolution of ε-caprolactam is generally explained by aminolysis and acidolysis via intra- and/or inter-molecular reactions [29].

Kashiwagi et al. [17] suggested that the reduction in PHRR is achieved by the formation of protective floccules on the sample surface which mainly consist of stacked clay layers, like the barrier effect mentioned above. Dabrowski et al. [30] showed that protective barriers slow the rate of degradation via a diffusion process and lower the escape of fuel. Pramoda et al. [31] compared the thermal degradation of the nanocomposite with that of virgin polyamide 6, using TGA/FTIR, and concluded that the presence of clay does not appear to have any effect on the degradation pathway of polyamide 6.

In this laboratory, GC/MS as well as TGA/FTIR have been used to study the degradation pathway of polymer–clay nanocomposites. In situ vapor phase FTIR only provides functionality information about the evolved gas products and structural changes cannot be identified. Thus, GC/MS analysis on the evolved products has also been performed, along with analysis of the solid residues. Using this method, the changes in the degradation pathway due to the barrier effect of clay were well elucidated for nanocomposites of polystyrene(PS)–clay [32] and ethylene vinylacetate copolymers(EVA)–clay [33]. In the presence of clay, it was concluded that the radicals produced during thermal degradation are momentarily contained by the clay and this permits radical recombination reactions to occur.

Considering the large reduction in PHRR of polyamide 6–clay nanocomposite, which is about the same as that of PS and EVA nanocomposites, it is believed that the degradation pathway of polyamide 6 must be modified in the presence of clay. Therefore, the degradation pathway of polyamide 6–clay nanocomposites was studied, using the same techniques as in the previous work [32,33].

2. Experimental

2.1. Materials and preparation of nanocomposite

Polyamide 6 (PA 6), purchased from the Aldrich Chemical Company, and the organically modified monmorillonite clay (Cloisite 30B, cation is methyl tallow bis(2-hydroxyethyl) ammonium), supplied by Southern Clay Products Inc., were used as received for the melt blending. Polyamide 6 and modified clay were melt blended in a Brabender Mixer at 60 rpm for 10 min at 230–240 °C, with the inorganic clay content ranging between 0.1 and 5.0 wt%.

2.2. Characterization of nanocomposite

Cone calorimetry and X-ray diffraction (XRD) were used to characterize the formation of nanocomposites. Cone calorimetry was performed on an Atlas CONE2 according to ASTM E 1354 at a heat flux of 35 kW/m^2, which is a normal irradiance level for the evaluation of the fire retardancy of polymers, using a cone shaped heater. Exhaust flow rate was 24 L/s and the spark was continuous until the sample ignited. The specimens for cone calorimetry were prepared by the compression molding of the sample (about 30 g) into $3 \times 100 \times 100$ mm^3 square plaques. Typical cone calorimetry results are reproducible within $\pm 10\%$. XRD patterns were obtained using a Rigaku Geiger Flex, 2-circle powder diffractometer equipped with Cu K$_\alpha$ generator ($\lambda = 1.5404$ Å); generator tension was 50 kV and the current was 20 mA.

2.3. TGA/FTIR analysis and sampling of evolved products

TGA/FTIR was carried out on a Cahn TG 131 instrument which was connected to a Mattson research grade FTIR through stainless steel tubing. The temperature reproducibility of the TGA is ± 3 °C and error range of non-volatile fraction at 700 °C is $\pm 3\%$. The thermal degradation in the TGA was carried out at a heating rate of 20 °C/min and a nitrogen flow of 80 ml/min. The sample size was 40–60 mg for the TGA evaluation; the sample cup of this instrument is quite large and this sample size does not in any way fill it. During thermal degradation in the TGA, the evolved volatile products are introduced to the IR chamber through a sniffer tube and stainless steel tubing and in situ vapor phase FTIR spectra are collected; this sniffer tube extends into the sample cup in the TGA and removes the evolved products at a rate of 40 ml/min. The temperature of the tubing was maintained at 300 °C. The evolved products during thermal degradation of each sample were collected using a cold trap at a temperature of -78 °C for the GC/MS analysis of the degradation products.

2.4. Analysis of evolved condensable products

The condensable evolved products in the trap were dissolved in acetonitrile and GC/MS spectra were obtained using a Agilent 6850 series GC connected to a Agilent 5973 series MS (70 eV ionization energy) with temperature programming from 40 to 250 °C. The identity of the evolved compounds was primarily established by co-injection with authentic compounds and/or by the analysis of mass fragmentation pattern. For the molecular ions that are difficult to assign via the above methods, they are assigned speculatively according to the known degradation pathway of polyamide 6.
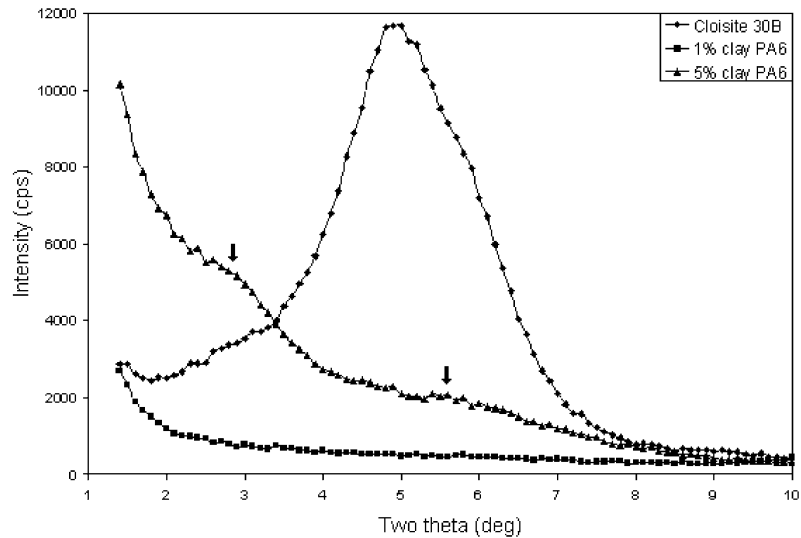
Fig. 1. XRD patterns for the modified clay (Cloisite 30B), 1% clay and 5% clay polyamide 6 nanocomposites.

2.5. Analysis of solid residue sample

The solid residues after 40% mass loss were collected. Viscosity measurements for the soluble fraction of residues were performed using an Ubbelodeh viscometer at the concentration of 0.100 g/10.0 ml of formic acid at 25.0 °C after separating the insoluble fraction. FTIR data were obtained for the solid residues using KBr pellets on a Nicolet Magna Model 560 spectrometer.

3. Results and discussion

3.1. The characterization of nanocomposite and thermal analysis

The XRD patterns of the modified clay and the polyamide 6 nanocomposites are shown in Fig. 1. The modified clay (Cloisite 30B) has a d-spacing of 2.1 nm and XRD data of 1% clay PA 6 sample exhibits the typical
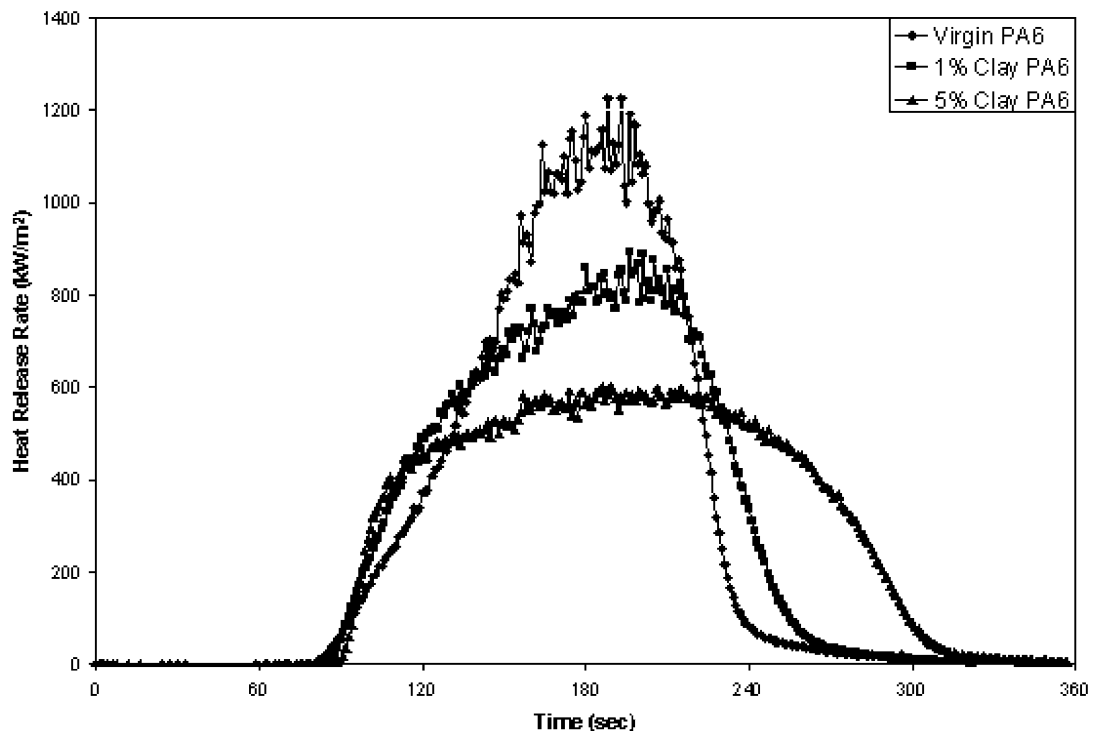

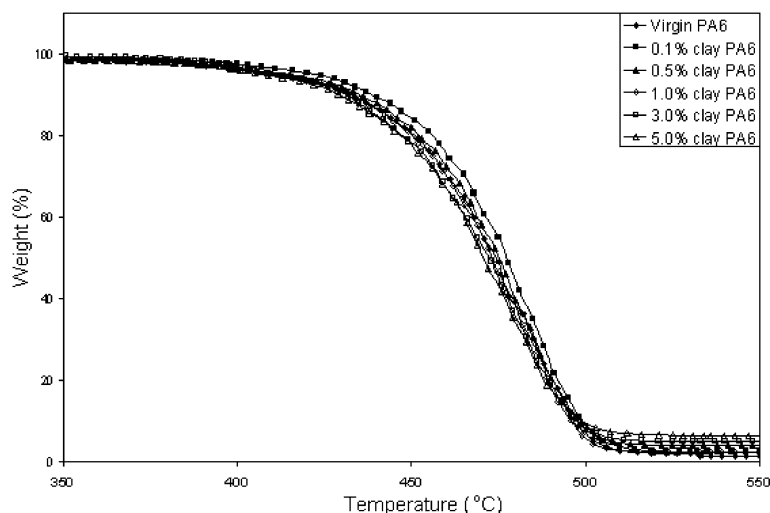Fig. 2. Heat release rate vs. time of PA 6 and PA 6–clay nanocomposites.

Fig. 3. TGA results of polyamide 6 and polyamide–clay nanocomposites.

pattern of well-dispersed and delaminated morphology. In the case of 5% clay PA 6 sample, because of the high loading of clay, small peaks at 2θ values of 2.8 and 5.6°, corresponding to (001) and (002) planes, respectively, were observed and a *d*-spacing of 3.2 nm was calculated. Below 5% clay the morphology is delaminated, but, when the clay level reaches 5%, a very small amount of intercalated morphology may be observed. Paul and co-workers have reported the absence of peaks in the XRD trace at ∼3% clay and complete delamination is seen in the TEM images [34]; the organically-modified clay with the quaternary cation having one alkyl tail leads to a well-delaminated morphology [35].

The heat release rate curves of virgin PA 6, 1% clay PA 6

and 5% clay PA 6 are shown in Fig. 2; this exhibits the typical fire performance behavior of polyamide 6 nanocomposites [17]. As the clay loading increases, the peak heat release rate (PHRR) decreases. The times to ignition of the nanocomposites are delayed by several seconds and there is no significant change in total heat released. This means that the entire polymer in the nanocomposite eventually burns. In the case of 5% PA 6 nanocomposite, the PHRR was reduced by 60%, compared to virgin PA 6. The same increase in the reduction in the peak heat release rate as the clay content increases that is shown in Fig. 2 has been previously reported [16,17].

The thermogravimetric analysis (TGA) curves of PA 6 and PA 6/clay nanocomposites are shown in Fig. 3. Pramoda
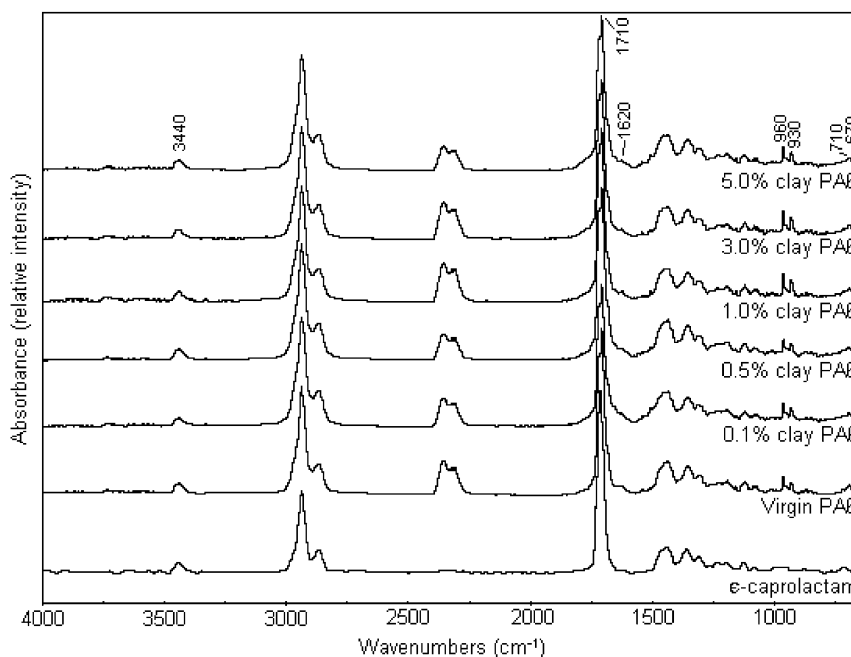

Fig. 4. In situ vapor phase FTIR spectra of polyamide 6 and polyamide 6–clay nanocomposites at 25% mass loss.
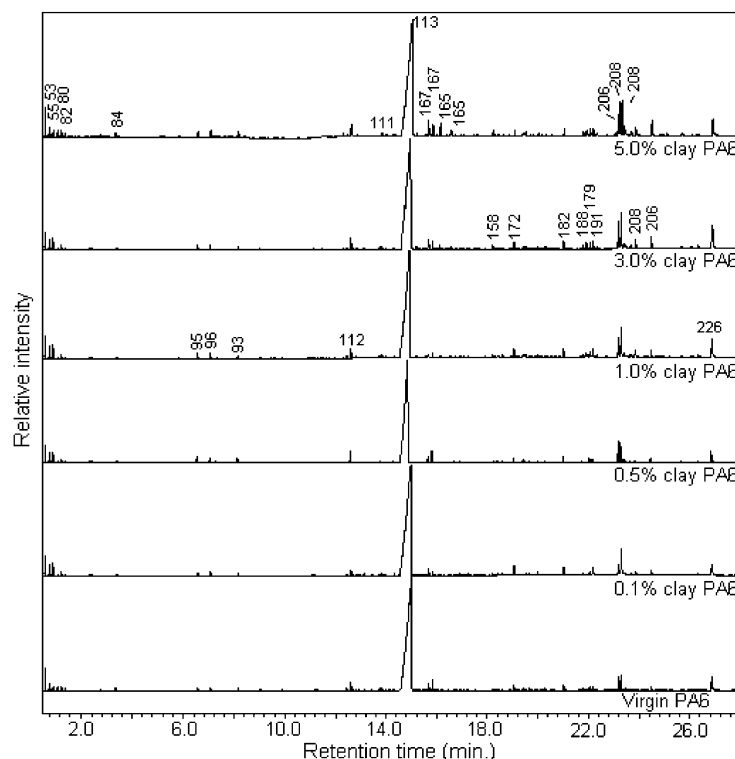
Fig. 5. GC traces for the evolved product of polyamide 6 and polyamide 6 nanocomposites. The inset numbers denote the molecular mass of the corresponding peak.

et al. [31] observed that the degradation onset temperature is 12 °C higher for PA 6 with 2.5% clay loading than that of virgin PA 6 and the onset temperature for the higher clay loading remained unchanged. On the other hand, similar TGA experiments on the PA 6 nanocomposites have been performed by other workers [17,30] and no significant changes were observed in the onset of degradation. In this study, the mass loss behavior of PA 6/clay nanocomposites is not significantly different from that of virgin PA 6. Irrespective of formulation, the temperatures at 50% mass loss are 471–476 °C, which is within the error range of the TGA instrument used in this study.

3.2. The analysis of the evolved products

The evolved products were analyzed using in situ vapor phase FTIR for each sample to monitor the functionality changes during thermal degradation. Fig. 4 shows the in situ vapor phase FTIR spectra at 25% mass loss. There is no significant difference between virgin PA 6 and PA 6 nanocomposites in terms of the peak positions, which means that the functionalities of the evolved products are the same for PA 6 and PA 6–clay nanocomposites, as previously shown by Pramoda et al. [31]. For comparison, the vapor phase FTIR of ε-caprolactam, which is the monomer of polyamide 6, is included in this figure. It is easily seen that most of the significant bands are due to ε-caprolactam; the band at 3440 cm^{-1} corresponds to nitrogen–hydrogen

stretching mode, the bands in the region of 2800–3000 cm^{-1} are caused by sp^3 carbon–hydrogen stretching, and the carbonyl band at 1710 cm^{-1} comes from amide group of ε-caprolactam.

Comparing the relative intensity in the carbon–hydrogen stretching region for polyamide 6 and polyamide 6–clay nanocomposites with that of ε-caprolactam, the peaks of the evolved products from polyamide 6 and polyamide 6–clay nanocomposites are more intense, implying that there are additional aliphatic compounds. It is not easy to see these intensities changes in the figure but, if one integrates the carbonyl peak at 1710 cm^{-1} relative to the C–H stretching vibration, the C–H band increases by about 20%. This trend is also observed for the nanocomposites as a function of clay loading. It appears that Pramoda et al. [31] did not note these small changes in the vapor phase FTIR.

As the clay loading increases, more intense bands in the aliphatic carbon–hydrogen stretching region are observed, as will be confirmed in the GC/MS results. The noise-like bands at 1400–1900 and 3500–3900 cm^{-1} are due to H$_2$O evolution, the shoulder-like band around 1620 cm^{-1} corresponds to the carbon–carbon double bond stretching, and the characteristic band of hydrogen cyanide is observed at 710 cm^{-1} in very low intensity. The diagnostic band of the nitrile group at 2250 cm^{-1} was not observed clearly because the products having nitrile group are not abundant and the sensitivity of nitrile band is relatively weak and probably overlapped with the carbon dioxide bands. The

Table 1
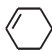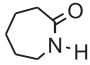The assigned structures for the peaks in GC traces

m/z	Time (min)	Structures
53	1.3	$H_2C=CH-CN$
55	1.4	H_3C-CH_2-CN
80	1.9	$H_2C=CH-CH=CH-CH=CH_2$
82	1.7	$H_2C=CH-CH=CH-CH_2-CH_2$
82	2.0	(cyclohexene ring structure)
84	3.8	$H_2C=CH-CH_2-CH_2-\overset{\overset{O}{\|}}{C}H$
93	8.4	$H_2C=CH-CH=CH-CH_2-CN$
95	6.6	$H_2C=CH-CH_2-CH_2-CH_2-CN$
96	7.1	$H_2C=CH-CH=CH-CH_2-\overset{\overset{O}{\|}}{C}H$
111	13.8	$H\overset{\overset{O}{\|}}{C}-(CH_2)_4-CN$
112	12.6	$H_2N-(CH_2)_5-CN$
113	15.1	(caprolactam ring with C=O and N-H)
158	18.2	$H_3C-\overset{\overset{O}{\|}}{C}-\overset{\overset{H}{\|}}{N}-(CH_2)_4-\overset{\overset{O}{\|}}{C}-NH_2$
165	16.2, 16.6	$H_2C=CH-CH=CH-CH_2-\overset{\overset{O}{\|}}{C}-\overset{\overset{H}{\|}}{N}-(CH_2)_2-CH=CH_2$
167	15.7, 15.9	$H_2C=CH-(CH_2)_2-\overset{\overset{O}{\|}}{C}-\overset{\overset{H}{\|}}{N}-(CH_2)_3-CH=CH_2$
172	19.1	$H_3C-\overset{\overset{O}{\|}}{C}-\overset{\overset{H}{\|}}{N}-(CH_2)_4-\overset{\overset{O}{\|}}{C}-\overset{\overset{H}{\|}}{N}-CH_3$
179	21.9	$H_2C=CH-CH=CH-CH_2-\overset{\overset{O}{\|}}{C}-\overset{\overset{H}{\|}}{N}-(CH_2)_3-CH=CH_2$
182	21.0	$CH_3-(CH_2)_2-\overset{\overset{O}{\|}}{C}-\overset{\overset{H}{\|}}{N}-(CH_2)_5-CN$
188	21.8	$H_2C=CH-CH=CH-\overset{\overset{O}{\|}}{C}-\overset{\overset{H}{\|}}{N}-CH_2-(CH=CH)_2-CN$
191	22.2	$H_2C=CH-CH=CH-\overset{\overset{O}{\|}}{C}-\overset{\overset{H}{\|}}{N}-(CH=CH)_2-CH_2-\overset{\overset{O}{\|}}{C}H$
206	23.2, 24.5	$H_2C=CH-CH=CH-CH_2-\overset{\overset{O}{\|}}{C}-\overset{\overset{H}{\|}}{N}-(CH_2)_5-CN$
208	23.2, 23.3, 23.9	$H_2C=CH-(CH_2)_3-\overset{\overset{O}{\|}}{C}-\overset{\overset{H}{\|}}{N}-(CH_2)_5-CN$
226	26.9	(cyclic diamide: $H-N-(CH_2)_5-C=O$ / $O=C-(H_2C)_5-N-H$)

Table 2
The percent integration of some significant peaks in GC traces

Sample	m/z 113 (%)	m/z 208 (%)	m/z 226 (%)	Others (%)
Virgin PA6	85.0	3.4	2.8	8.8
0.1% clay PA6	84.2	4.5	2.3	9.0
0.5% clay PA6	81.6	7.8	3.4	7.2
1.0% clay PA6	80.4	6.6	4.1	8.9
3.0% clay PA6	73.2	7.3	4.9	14.6
5.0% clay PA6	71.3	6.9	3.0	18.8

evolved products from the thermal degradation of polyamide 6 include carbon dioxide (2400–2200 and 670 cm^{-1}) [36] and ammonia (960 and 930 cm^{-1}) [31,36] in significant intensity.

In order to assign the structures of the evolved products, they were collected using a cold trap at $-78\,^\circ$C during thermal degradation and GC/MS analysis was carried out. Fig. 5 shows the GC traces of the collected evolved products. Since acetonitrile was used as the solvent for the collection of the evolved products, the mass spectra for each GC trace exhibit only molecular mass higher than about m/z 50. The structures were identified through the analysis of mass fragmentation pattern and/or by co-injection with authentic compounds; some structures are speculatively assigned according to the degradation patterns that were proposed by the previous workers [24–29]. The assigned structures are shown in Table 1, while Table 2 shows the percent integration results for some significant evolved

products, the error range, for the most abundant peak, ε-caprolactam, is $\pm 3\%$. As mentioned in the vapor phase FTIR results, the generation of ε-caprolactam was qualitatively decreased as the clay loading increases (Fig. 5). Table 2 also shows that the integration area of the ε-caprolactam (m/z 113, retention time 15.0 min) decreases with an increase in the clay loading. Thus, it is noted that the degradation pathway of polyamide 6 has been affected by the presence of clay, which was not detected by the previous workers [17,30,31]. The relative intensity of other compounds, except ε-caprolactam, increases as the clay loading increases. No new structures are identified in the presence of clay, which supports the assertion that no functionality changes were observed in the vapor phase FTIR results (Fig. 4).

As mentioned in the vapor phase FTIR discussion, some changes were observed in the region of the sp^3 carbon–hydrogen stretching mode. Many of the assigned structures
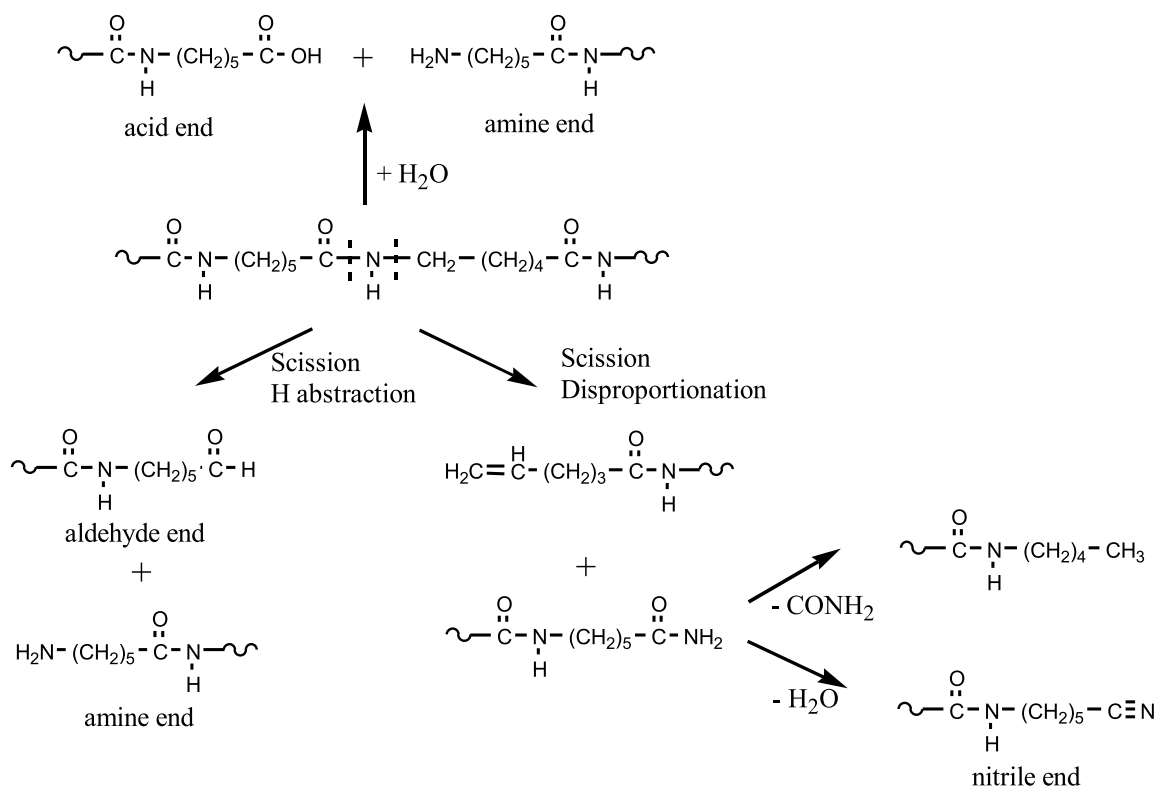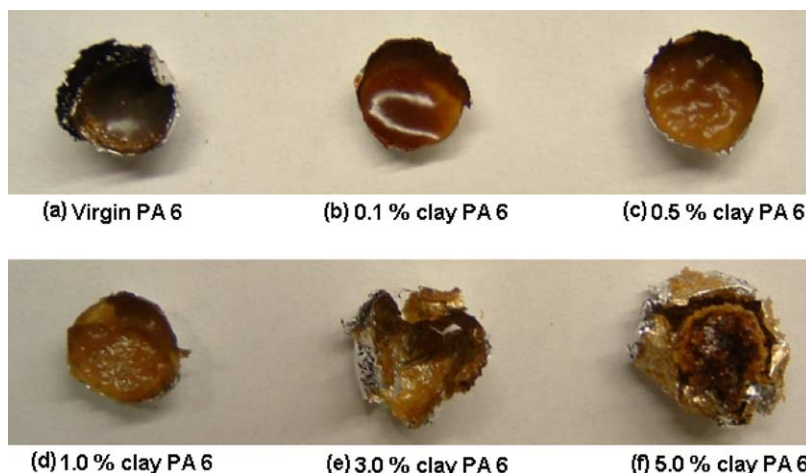

Scheme 1.

Fig. 6. Residue pictures of polyamide 6 and polyamide 6 nanocomposites after 40% mass loss.

exhibit a smaller fraction of carbonyl, compared to ε-caprolactam (*m/z* 113, 15.0 min) and its dimer (*m/z* 226, 26.9 min), and some aliphatic structures with no carbonyl groups are assigned, as shown in Table 1. Thus, the increase of other structures in the GC/MS may explain why the relative intensity of the sp^3 carbon–hydrogen stretching mode increases in the presence of clay.

Many small molecules, including aliphatic structures, have been previously identified [37–39]. Considering the end groups in the linear structures in Table 1, many structures have nitrile and unsaturated aliphatic chain ends. The mechanism of the formation of these end groups will be shown in Scheme 1. For the *m/z* of 165, 167, 206 and 208, it appears that isomers having different structures are present, but one representative structure for each *m/z* is shown, based on the degradation pathway of polyamide 6.

Through the analysis of the evolved products using FTIR and GC/MS, some quantitative differences are observed. Vapor phase FTIR shows relatively more intense bands in

the aliphatic carbon–hydrogen stretching mode and the GC traces reveal that monomer evolution decreases as the clay loading increases. The vapor phase FTIR result is qualitatively similar to the work done by Promoda et al. [31] in terms of functionality information. Since these changes in the vapor phase FTIR and GC/MS necessarily imply some changes in the condensed phase, analysis of the solid residues was carried out.

3.3. Analysis of solid residue samples after 40% mass loss

The residues after 40% mass loss were collected and photographs of them are shown in Fig. 6. Virgin PA 6 (a) and 0.1% clay PA 6 nanocomposite (b) show a smooth surface; as the clay loading increases, the surface becomes rough, as shown in Fig. 6(c) and (d), and finally forms an expanded net-like structure, as shown in Fig. 6(e) and (f). The 5% clay polyamide 6 appears to exhibit a typical intumescent morphology at 40% mass loss. Since the clay
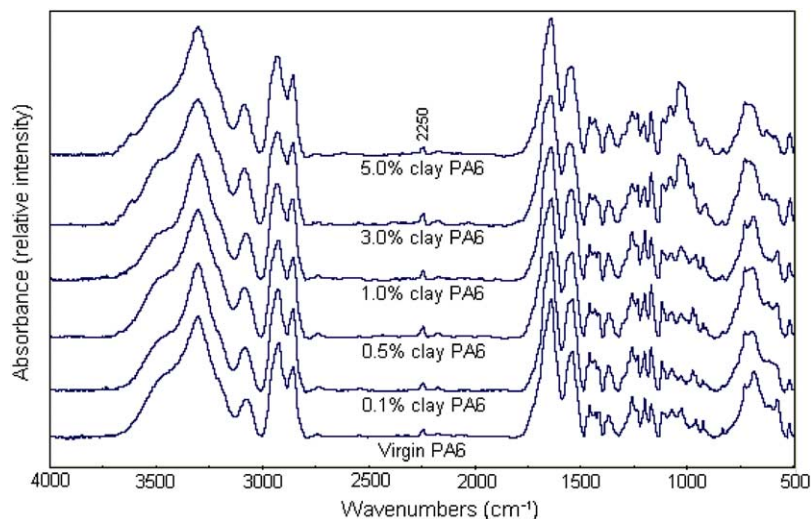

Fig. 7. FTIR spectra of solid residues at 40% mass loss after making KBr pellet.
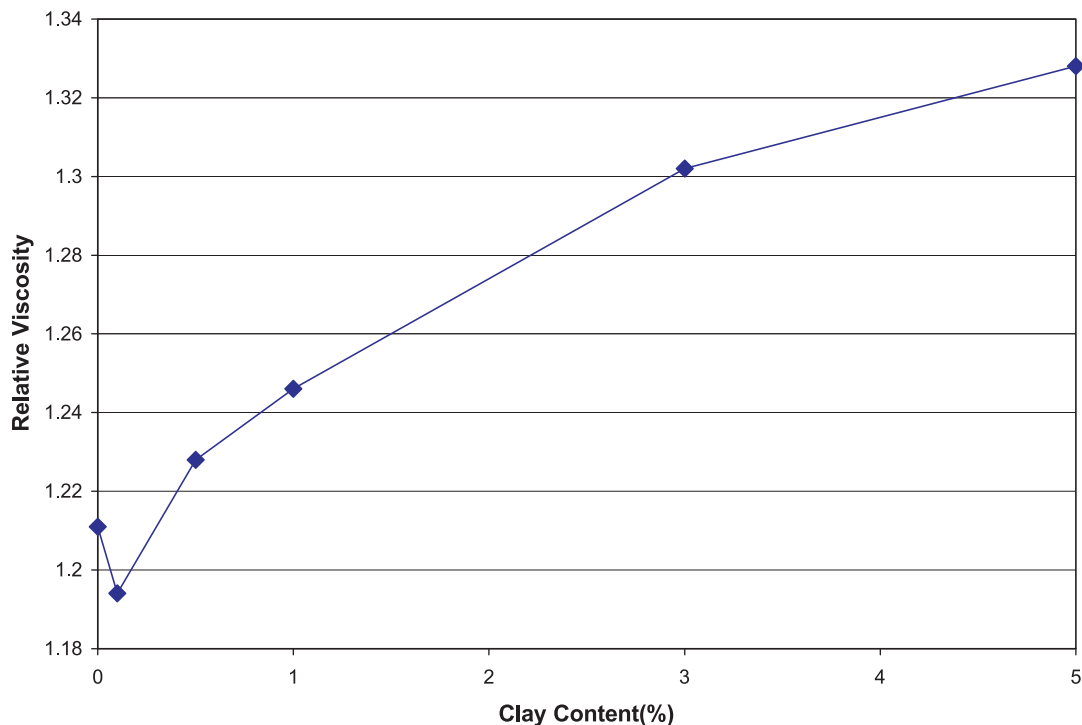
Fig. 8. Relative viscosity as a function of clay content at 40% mass loss of samples.

shows good compatibility with polyamide, probably because of hydrogen bonding, it appears that the clay layers form a net-like structure with the degrading polyamide 6, causing an increase in the free volume of the interior. It can be assumed from this result that inter-molecular reactions occur between degraded molecules from polyamide 6. However, these organic products eventually decompose, as can be seen in the TGA and cone results.

It was proposed that the clay layers form the island-like floccules instead of forming a continuous net-like structure [17]. In this study, the swelled net-like structure was observed for the 5% clay PA 6 sample, as shown in Fig. 6(f). It is thought that this difference arises due to the differences in the test conditions; Kashiwagi et al. [17] carried out thermal degradation in a cone calorimeter at 50 kW/m^2, which puts the sample instantly at very high temperature, while this study was carried out by gradual heating at a ramp rate of 20 °C/min. Thus, the mass loss and degradation rate at 50 kW/m^2 is so large that the clay layers migrate to the surface as bubbles of degrading molecules and accumulate

at the surface in a very short time, and the degrading polyamide 6 has little opportunity to form a net-like structure with the clay layers. Michal et al. [39] and Holland et al. [26,40] showed that the amount of non-volatile residue decreased with increasing degradation temperature (isothermal conditions).

FTIR spectra were obtained for the above residues, but no changes were observed, except the band at 1020 cm^{-1}, which is due to silicon–oxygen stretching, as shown in Fig. 7. The FTIR spectra of the residues of nanocomposites at 40% mass loss are similar to those of virgin polyamide 6 at 40% mass loss, which means that the same functionalities are present. The nitrile band (2250 cm^{-1}), which could not be detected in the FTIR of the vapor phase, because the band is very weak and overlapped with the bands of CO_2 and CO, is observed in the condensed phase FTIR of the solid residue for all samples, but it is not present for the non-degraded polyamide 6. It can be assumed that the nitrile groups arise during degradation; they are also present in some structures of the evolved products, as shown in Table 1.
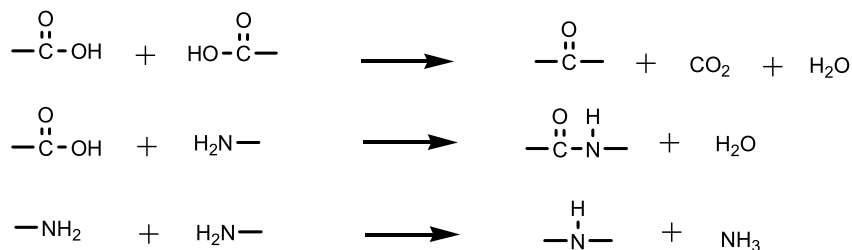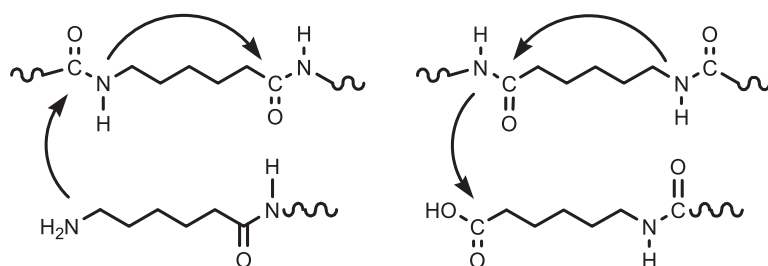

Scheme 2.

Intramolecular Aminolysis/Acidolysis
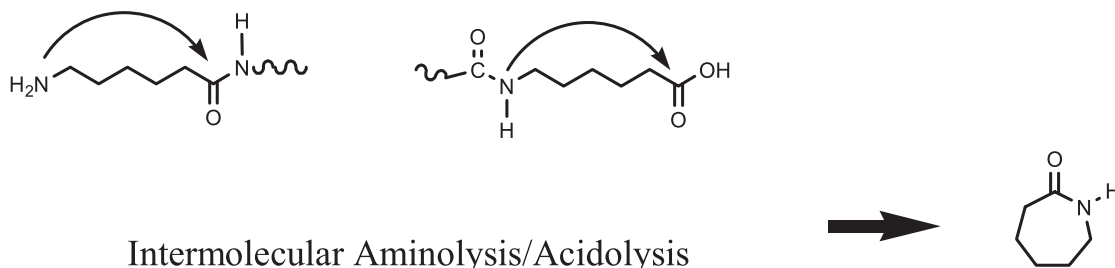
Intermolecular Aminolysis/Acidolysis

Scheme 3.

By incorporating clay into polyamide 6, the appearance of solid residues has changed significantly. In order to see if there is a change in molecular weight, viscosity was measured for the soluble fractions of each residue sample and the results are shown in Fig. 8. The organic portion of the residue that was insoluble in formic acid was 5–8%, irrespective of formulation (the residue expected from clay is subtracted to give the organic portion). The viscosity decreases initially and then increases with increasing clay content, which means that the residues of polyamide 6–clay nanocomposite having higher clay content have a higher molecular weight. It has been noted that degradation occurs during processing of polyamide 6/clay nanocomposites due to hydrolysis of the amide linkage [29], which may explain the viscosity decrease for the residue of 0.1% clay polyamide 6 nanocomposite. The higher viscosity for solid residues of the nanocomposites after 40% mass loss is ascribed to the presence of the clay.

3.4. Degradation pathway of polyamide 6 and polyamide 6/clay nanocomposite

The thermal degradation pathway for polyamide 6 was reviewed by Levchik et al. [25] and some important pathways were systemically organized by Davis et al. [29]. The thermal degradation pathway of polyamide 6 described in this study was mainly extracted from these two studies. Scheme 1 shows how the end groups are generated for the linear structures in the evolved products. The assigned structures in Table 1, except monomer and dimer, generally follow Scheme 1. The pathway for the evolution of ammonia, water and carbon dioxide is explained by the secondary reaction, shown in Scheme 2. Hydrogen abstraction occurs during the thermal degradation, producing additional double bonds in the chain, as evidenced in m/z 93, 96, 179, 206, etc.

The most dominant species in the evolved products is ε-caprolactam (m/z 113, 15.1 min), the monomer of polyamide 6. This can be produced through intra- and/or inter-molecular aminolysis/acidolysis reaction, as shown in Scheme 3. The dimer (m/z 226, 26.9 min) is produced in a similar fashion. It is generally accepted that monomer formation is primarily generated by intra-molecular reactions rather than inter-molecular reactions [29].

In the presence of clay, the soluble fractions of PA 6–clay nanocomposite show increased viscosity and this increase can be explained by inter-molecular reactions since one chain attacks another, leading to larger molecules. The clay provides more opportunity for degrading polyamide 6 to undergo intermolecular aminolysis/acidolysis by containment of the degrading polymer.

In the GC/MS results, the relative intensity of ε-caprolactam decreased with increasing clay content (Fig. 5). Except for monomer and dimer, many evolved structures are produced via chain scission. This result implies that the evolved products via chain scission also increase during thermal degradation of polyamide 6 in the presence of clay.

4. Conclusions

Vapor phase in situ FTIR gives no significant differences in the evolved products during the thermal degradation for virgin polyamide 6 and polyamide 6–clay nanocomposites

in terms of functionality, but changes in the relative intensity in the carbon–hydrogen stretching region with the clay loading are observed. The decrease in relative intensity in the ε-carprolactam (GC/MS) supports the vapor phase FTIR result. The pathway of ε-carprolactam generation is aminolysis and/or acidolysis through intra- or inter-chain reaction. As the clay loading is increased, the viscosity of solid residue is increased. Thus, it is concluded that inter-molecular reactions become significant due to the barrier effect of the well-dispersed clay, which causes the formation of larger molecules. The clay contains the degrading polymer and this containment permits the occurrence of radical recombination or inter-chain reactions. These changes in the degradation pathway may relate to the significant reduction in the peak heat release rate.

References

[1] Alexandre M, Dubois P. Mater Sci Eng 2000;R28:1–63. Ray SS, Okamoto M. Prog Polym Sci 2003;28:1539–641.

[2] Kojima Y, Usuki A, Kawasumi M, Okada A, Fukushima Y, Karauchi T, et al. J Polym Sci, Part A: Polym Chem 1993;31:983–6.

[3] Zhu J, Morgan AB, Lamelas FJ, Wilkie CA. Chem Mater 2001;13:3774–80.

[4] Bourbigot S, Gilman JW, Wilkie CA. Polym Degrad Stab 2004;84:483–92.

[5] Kato C, Kuroda K, Misawa M. Clays Clay Miner 1979;27:129–36.

[6] Okada A, Kawasumi M, Kurauchi T, Kamigaito O. Polym Prep 1987;28:447–8.

[7] Usuki A, Kojima Y, Kawasumi M, Okada A, Fukushima Y, Kurauchi T, et al. J Mater Res 1993;8:1179–84.

[8] Kojima Y, Usuki A, Kawasumi M, Okada A, Kurauchi T, Kamigaito O. J Polym Sci Polym Chem 1993;31:1755–8.

[9] Okada A, Kawasumi M, Usuki A, Kojima Y, Kurauchi T, Kamigaito O. Mater Res Soc Symp Proc 1990;171:45–50.

[10] Kojima Y, Usuki A, Kawasumi M, Okada A, Kurauchi T, Kamigaito O. J Polym Sci Polym Chem 1993;31:983–6.

[11] Kojima Y, Usuki A, Kawasumi M, Okada A, Fukushima Y, Kurauchi T, et al. J Mater Res 1993;8:1185–9.

[12] Kojima Y, Usuki A, Kawasumi M, Okada A, Kurauchi T, Kamigaito O. J Appl Polym Sci 1993;49:1259–64.

[13] Kojima Y, Usuki A, Kawasumi M, Okada A, Kurauchi T, Kamigaito O. Materiaru Raifu (Japan) 1993;5:13–17.

[14] Liu T, Tjiu WC, He C, Na SS, Chung TS. Polym Int 2004;53:392–9.

[15] Rhutesh K, Paul DR. Polymer 2004;45:2991–3000.

[16] Gilman JW, Kashiwagi T, Giannelis ET, Manias E, Lomakin S, Lichtenhan JD, et al. In: Le Bras M, Camino G, Bourbigot S, Delobel R, editors. Fire retardancy of polymers the use of intumescence. Cambridge, UK: Woodhead Publisher; 1998. p. 203–21.

[17] Kashiwagi T, Harris Jr RH, Zhang X, Briber RM, Cipriano BH, Raghavan SR, et al. Polymer 2004;45:881–91.

[18] Gilman JW, Jackson CL, Morgan AB, Harris R, Manias E, Giannelis EP, et al. Chem Mater 2000;12:1866–73.

[19] Zhu J, Uhl FM, Morgan AB, Wilkie CA. Chem Mater 2001;13:4649–54.

[20] Wang J, Du J, Zhu J, Wilkie CA. Polym Degrad Stab 2002;77:249–52.

[21] Du J, Zhu J, Wilkie CA, Wang J. Polym Degrad Stab 2002;77:377–81.

[22] Du J, Wang J, Su S, Wilkie CA. Polym Degrad Stab 2004;83:29–34.

[23] Du J, Wang D, Wilkie CA, Wang J. Polym Degrad Stab 2002;77:249–52.

[24] Dussel HJ, Rosen H, Hummel O. Makromol Chem 1976;177:2343–68.

[25] Levchik SV, Weil ED, Lewin M. Polym Int 1999;48:532–57.

[26] Holland BJ, Hay JN. Polym Int 2000;49:943–8.

[27] Herrera M, Matuschek G, Kettrup A. J Therm Anal Cal 2000;59:385–94.

[28] Herrera M, Matuschek G, Kettrup A. Chemosphere 2001;42:601–7.

[29] Davis RD, Gilman JW, VanderHart DL. Polym Degrad Stab 2003;79:111–21.

[30] Dabrowski F, Bourbigot S, Delobel R, Le Bras M. Eur Polym J 2000;36:273–84.

[31] Pramoda KP, Liu T, Liu Z, He C, Sue HJ. Polym Degrad Stab 2003;81:47–56.

[32] Jang BN, Wilkie CA. Polymer (in press).

[33] Costache M, Wilkie CA. Polym Mater Sci Eng 2004;91:30–1.

[34] Fornes TD, Yoon PJ, Hunter DL, Keskkula H, Paul DR. Polymer 2002;43:5915–33.

[35] Fornes TD, Hunter DL, Paul DR. Macromolecules 2004;37:1793–8.

[36] Pouchert CJ. The Aldrich library of FT-IR spectra. 1st ed. Vapor phase 1985. Aldrich Chemical Company, Milwaukee, WI.

[37] Braun E, Levin BC. Fire Mater 1987;11:71–88.

[38] Straus S, Wall LA. J Res Nat Bur Stand 1958;60:39–45.

[39] Michal J, Mitera J, Kubat J. Fire Mater 1981;5:1–5.

[40] Holland BJ, Hay JN. Polymer 2001;42:4759–61.